Photoinduced Reactivity of Strongly Coupled TiO2 Ligands Under Visible Irradiation: An Examination of an Alizarin Red@TiO2 Nanoparticulate System

ARTICLE *in* THE JOURNAL OF PHYSICAL CHEMISTRY C · AUGUST 2008

Impact Factor: 4.77 · DOI: 10.1021/jp8040742

4 AUTHORS:

Yesica di iorio
INTEMA instituto de Investigaciones en Cie…
11 PUBLICATIONS **95** CITATIONS
SEE PROFILE

Enrique San Román
University of Buenos Aires
60 PUBLICATIONS **1,024** CITATIONS
SEE PROFILE

Marta I Litter
Comisión Nacional de Energía Atómica
143 PUBLICATIONS **4,618** CITATIONS
SEE PROFILE

María A. Grela
Universidad Nacional de Mar del Plata
55 PUBLICATIONS **1,095** CITATIONS
SEE PROFILE

THE JOURNAL OF PHYSICAL CHEMISTRY C

Article

Photoinduced Reactivity of Strongly Coupled TiO Ligands under Visible Irradiation: An Examination of an Alizarin Red@TiO Nanoparticulate System

Yesica Di Iorio, Enrique San Roma#n, Marta I. Litter, and Mari#a A. Grela

J. Phys. Chem. C, **2008**, 112 (42), 16532-16538 • DOI: 10.1021/jp8040742 • Publication Date (Web): 25 September 2008

Photoinduced Reactivity of Strongly Coupled TiO_2 Ligands under Visible Irradiation: An Examination of an Alizarin Red@TiO_2 Nanoparticulate System

Yesica Di Iorio,[†] Enrique San Román,[‡] Marta I. Litter,[§,||] and María A. Grela*[,†]

Departamento de Química, Universidad Nacional de Mar del Plata, Funes 3350, B7602AYL Mar del Plata, Argentina, INQUIMAE, Facultad de Ciencias Exactas y Naturales, Ciudad Universitaria, Pabellón 2, 1428 Buenos Aires, Argentina, Gerencia Química, Comisión Nacional de Energía Atómica, Av. Gral. Paz 1499, 1650 San Martín, Prov. de Buenos Aires, Argentina, and Escuela de Posgrado, Universidad de Gral. San Martín, Peatonal Belgrano 3563, 1er. piso, 1650 San Martín, Prov. de Buenos Aires, Argentina

Received: May 8, 2008; Revised Manuscript Received: August 1, 2008

Similarly to alizarin molecules, 3,4-dihydroxy-9,10-dioxo-2-anthracenesulfonate (alizarin red, AR), chelates TiO_2 nanoparticles through the catechol moiety, and shifts the absorption threshold of the semiconductor to the visible region. The photoinduced reactivity of the coupled system AR@TiO_2 was investigated through quantum yields determinations in nonscattering sols of TiO_2 modified nanoparticles. In contrast with the behavior observed in TiO_2 microparticulated systems, the chemisorbed ligand has a high stability under aerated visible light irradiation. The quantum yield for alizarin red oxidation $\Phi_{-AR} = 4 \times 10^{-4}$ correlates with the negligible efficiency for oxygen reduction in the constrained environment of the smaller particles. Conversely, reduction of Cr(VI) to Cr(V) in the coupled AR@TiO_2 system, confirmed by electron paramagnetic resonance spectroscopy, utilizes a high fraction of the photogenerated electrons and induces the degradation of the complex. Quantum efficiencies for chromium(VI) disappearance, $\Phi_{-Cr(VI)}$, approaches 37% at $[Cr(VI)]_0 = 200\ \mu M$. The interactions between Cr(VI)/AR and Cr(VI)/TiO_2 are analyzed in detail. Spectroscopic evidence is presented for the first time that Cr(VI) forms a charge-transfer complex with TiO_2 nanoparticles that could be excited by visible light ($\lambda \leq 440$ nm). The environmental implications of the above findings are briefly discussed.

Introduction

Surface modification of TiO_2 nanosized particles with organic ligands is an active area of research due to its relevance in environmental remediation, solar energy conversion, and the development of electrochromic and artificial photosynthetic devices.[1−5]

Nearly two decades ago, Grätzel et al. reported that surface chelation of titanium dioxide particles by some monodentate and bidentate organic ligands produces colored complexes and accelerates the rate of reduction of methyl viologen by conduction band electrons.[6,7] After that, Rajh and co-workers demonstrated that the strong interaction between enediol ligands and titanium dioxide nanoparticles results in the adjustment of the coordination geometry of surface Ti atoms[8] and the displacement of inter-band-gap states into the conduction band.[8,9] More interesting, the onset of absorption of the coupled enediol systems exhibits a significant shift to the visible region compared to the unmodified particles, which correlates with the dipole moment of the surface bound Ti−ligand composite. However, most of the research dealing with surface complexes has mainly focused on their photochemical behavior under UV irradiation,[10] and only recently, their photoactivity by visible light excitation has been investigated.[11−13] The widespread use of highly dispersive concentrated suspensions of TiO_2 microparticles may have obscured the visual detection of the charge-transfer complexes, which nevertheless were extensively characterized by IR spectroscopy.[14] It has been proven that relatively large polycrystalline TiO_2 particles having both rutile and anatase phases facilitate the formation of surface bound complexes.[11] However, as the size of the particles gets into the nanometer domain, the fraction of undercoordinated atoms located at the surface increases, and thus, the reactivity toward binding is deeply enhanced.[8]

Comprehensive ultrafast laser studies on the electron-transfer dynamics of strongly coupled ligand/semiconductor colloidal systems have shown that the forward (molecule to semiconductor) electron-transfer process can be extremely rapid, in the range 1−100 fs, while the back reaction is generally nonexponential and spans over various time decades (from picoseconds to microseconds).[15−18] The accumulated evidence indicates that a high proportion of the recombination processes takes place in the subnanosecond region probably involving geminate pairs. Nevertheless, it has been reported that some of the carriers recombine with much slower characteristic times,[19] but the fraction of these pairs that are able to engage in interfacial redox reactions remains elusive.[20,21]

Among catecholate ligands, alizarin represents an interesting and intriguing molecule exhibiting a large spectral red shift ($\lambda \sim 70$ nm) when complexing the Ti atoms in TiO_2. Experimental evidence[15,16] and theoretical studies[22] have demonstrated that charge injection is not the result of a direct charge-transfer transition but proceeds extremely fast ($\tau = 6$ fs) from the photoexcited state of the ligand, which is located near the conduction band of the oxide. Thus, this molecule has attracted a lot of attention as a model for interrogating the basic aspects of the dynamics of interfacial electron-transfer processes.

* Author to whom correspondence should be addressed. E-mail: magrela@mdp.edu.ar.
[†] Universidad Nacional de Mar del Plata.
[‡] Ciudad Universitaria.
[§] Comisión Nacional de Energía Atómica.
[||] Universidad de Gral. San Martín.

10.1021/jp8040742 CCC: $40.75
Published on Web 09/25/2008

SCHEME 1: Chemical Structure of AR: The Sensitizing Ligand

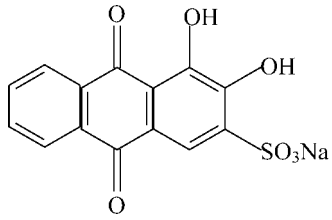

Moreover, injection near the edge of the conduction band implies optimal utilization of the excitation energy in solar cells, avoiding energy wasting processes.[22]

In this paper, we focus on the photochemical redox performance of aqueous colloid sols of TiO_2 nanoparticles coupled to the soluble derivative of alizarin, 3,4-dihydroxy-9,10-dioxo-2-anthracenesulfonate, containing only a minor (negligible) fraction of the free ligand in solution. In the following, we (i) analyze the stability of this system under visible irradiation and (ii) scrutinize the possible utilization of the photoinduced species: electrons and AR^+ in selected redox processes.

Experimental Section

Chemicals. All chemicals were of the highest purity available. AR, (Scheme 1), was purchased from Sigma-Aldrich and used as received. Hydroquinone (Merck) and 1,4-benzoquinone (Aldrich) were recrystallized from benzene, and their solutions were freshly prepared before use.[23] Phenylglyoxylic acid (Sigma) was recrystallized from carbon tetrachloride (Merck). $KCr(NH_3)_2(NCS)_4$ was prepared from the Reinecke salt[24] (Aldrich) and recrystallized from warm water as described.[24]

All solutions were prepared using ultrapure water (resistivity 18 MΩ cm). $HClO_4$ (Merck, p.a. 60%) was used to adjust the pH throughout, since perchlorate anions are not expected to adsorb specifically. Titanium tetraisopropoxide (99.999%, Aldrich) and 2-propanol (Merck) were used in the synthesis of amorphous colloidal TiO_2.

Preparation of Colloidal TiO_2 Nanoparticles. Colloidal TiO_2 was prepared by controlled acid hydrolysis of titanium tetraisopropoxide following standard procedures.[25] Briefly, 1 cm^3 of $Ti[OCH(CH_3)_2]_4$ was dissolved in 20 cm^3 of 2-propanol and slowly added to an aqueous $HClO_4$ solution (200 cm^3, pH = 1.5) maintained at 1 °C. The solution was continuously stirred in the dark for 48−72 h, to promote aging and a more stable and uniform size distribution.[26] After this period, the solutions were concentrated at 35 °C under vacuum in a rotary evaporator. X-ray diffraction analysis, performed on a Philips X-Pert PW-3710 diffractometer using Cu Kα radiation ($\lambda = 0.154056$ nm), reveals that the nanoparticles have an amorphous structure with a small proportion of anatase.[27]

Sols of TiO_2 modified particles, hereafter AR@TiO_2, were prepared by addition of appropriate amounts of an aqueous acidified AR stock solution to a TiO_2 sol, under vigorous stirring.

Characterization Techniques. UV−vis absorption spectra were recorded with an Ocean Optics diode array fiber optics spectrophotometer.

The infrared measurements were performed on a Perkin-Elmer Fourier transform spectrophotometer model Spectrum BX equipped with a DTGS detector and a HATR unit with a horizontal 45 ° ZnSe crystal. Spectra are the average of 200 scans taken at 4 cm^{-1} resolution versus the appropriate single-beam background spectrum. TiO_2 films were coated onto an area of 4 cm × 1 cm of the ZnSe crystal by applying 100 μL of a 0.1 M TiO_2 sol. After drying in air overnight, the films were derivatized by applying 20 μL of a 1 mM AR solution to the oxide layer.

Cyclic voltammograms were performed with a Princeton Applied Research (PAR) model 173 potentiostat/galvanostat, and a PAR model 175 universal programmer, and recorded on a Velleman "PCS500AU" PC based digital storage oscilloscope interfaced to a personal computer. The electrochemical cell was a standard three-compartment cell with a Pt foil (2 cm^2) as counterelectrode, and glassy carbon and Ag/AgCl as working and reference electrodes, respectively. The electrochemical experiments were carried out at room temperature (25 °C) under N_2 atmosphere. AR was dissolved in a 0.1 M tetrabutylammonium perchlorate (TBAP) solution in acetonitrile to obtain a final concentration, [AR] = 1 mM.

Electron paramagnetic resonance experiments were performed at 298 K with a Bruker ER 200 X-band spectrometer. Calibration of the EPR instrument, data acquisition, and calculations of *g*-values are described elsewhere.[28] Typical data acquisition parameters were the following: data points, 2K; central field, 3510 G; sweep width, 100 G; scans 1−20; microwave power, 43 mW; modulation frequency, 100 kHz; time constant, 0.5−2 ms; sweep time, 0.5−2 s; modulation amplitude, 1.25 Gpp; receiver gain, 1.6×10^6; and attenuation, 7 dB.

General Procedures. Steady-state photolyses were performed with a high pressure Hg−Xe lamp coupled to a Kratos−Schoeffel monochromator, 5 nm bandwidth. Photolyses were carried out in 3 cm^3 square quartz prismatic cells (path length, $l = 1$ cm). Photon flux determinations were performed using appropriate chemical actinometers. Phenylglyoxylic acid ($\lambda \leq 400$ nm),[29] ferrioxalate[30] ($400 \leq \lambda/\text{nm} \leq 480$), or the potassium Reinecke salt[24] ($480 \leq \lambda/\text{nm} \leq 530$) were alternatively selected depending on the irradiation wavelength.

Incident photon fluxes, I_0 (s^{-1} m^{-2}), were 4.0×10^{17} and 1.9×10^{18} at 400 and 530 nm, respectively. To determine the dependence of the quantum yields on the irradiation intensity under UV and visible excitation, the direct photon emittance at two selected wavelengths, 303 and 480 nm, was attenuated with fine mesh metal screens of different transmittance. I_0 values spanned in these conditions the range $4.3 \times 10^{17} \leq I_0/s^{-1}\ m^{-2} \leq 1.32 \times 10^{19}$ and $1.7 \times 10^{17} \leq I_0\ /s^{-1}\ m^{-2} \leq 3.0 \times 10^{19}$ at 303 and 480 nm, respectively.

Absorbed light intensity at the irradiation wavelength was evaluated as $I_{a\lambda} = I_0 \times (1-10^{-A_\lambda})$ using the incident photon flux and the measured absorbance, A_λ. Typically, $A_\lambda \sim 0.35$.

Analysis. Changes in Cr(VI) concentration were followed by the diphenylcarbazide spectrophotometric method at 540 nm.[31] HPLC analysis was employed to quantify the evolution of hydroquinone and benzoquinone. The HPLC system consisted of a gradient pump equipped with a UV−vis photodiode array detector (UV2000-Thermo Separation Products), equipped with an ODS, 5 μm, 250 mm × 4.6 mm, Phenomex column. Methanol/water 25% by volume was used as eluent, and the detection was performed at $\lambda = 280$ nm.

Results and Discussion

Structure and Bonding of AR-Modified TiO_2 Nanoparticles. Figure 1 shows the changes in the absorption spectrum of an aqueous 40 μM solution of AR, at pH 1.5, after the addition of variable amounts of TiO_2 nanoparticles. As previously observed for 1,2-dihydroxy-9,10-anthraquinone (alizarin, A), the addition of TiO_2 to the AR solution shifts the spectrum of the dye to the red and considerably increases the molar extinction coefficient of the visible band. Experimental and

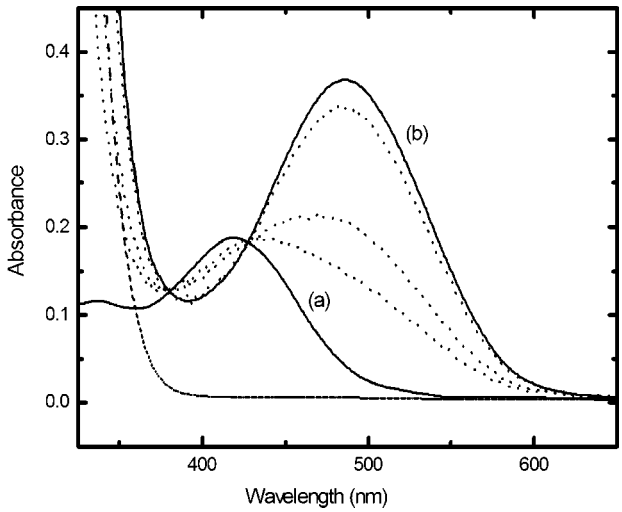

Figure 1. Changes in the absorption spectra of an aqueous 40 μM AR solution at pH 1.5 after the addition of variable amounts of TiO_2 nanoparticles. Solid lines refer to the spectra for (a) $[TiO_2] = 0$ and (b) $[TiO_2] \geq 4.5$ mM. Dotted lines show the dye absorption after progressive modification with $[TiO_2] = 0.27$, 0.40, and 1.0 mM. Dashed line is the spectrum of a 4.5 mM naked sol of TiO_2 nanoparticles.

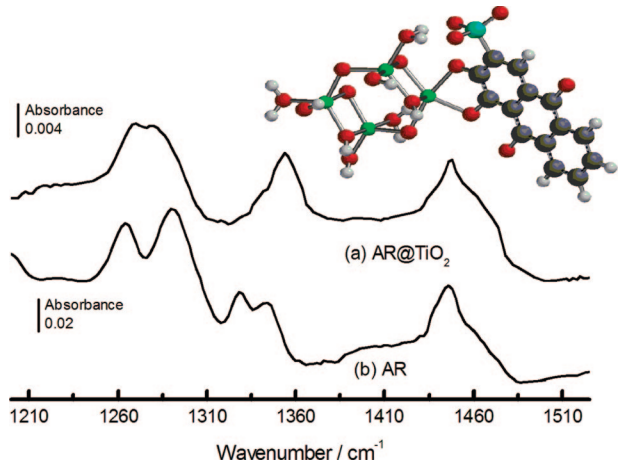

Figure 2. ATR-IR spectra for (a) AR@TiO_2 and (b) free AR. For AR@TiO_2, the spectrum of the TiO_2 film prior to the derivatization step was taken as background. The FTIR spectra of an aqueous solution of AR was obtained for comparative purposes and band assignment. The proposed molecular structure of AR bound to a small TiO_2 cluster is schematically shown in the figure.

theoretical evidence indicates that the coupling of alizarin molecules to TiO_2 occurs through the two chelating OH groups of its catechol moiety to one surface Ti^{4+} ion.[15,32] For AR, the presence of the sulfonate group opens up a new possible interaction with the positively charged surface of the TiO_2 nanoparticles. However, as recently published, the ATR-IR spectrum of AR over a TiO_2 film and that of an aqueous solution of the ligand do not show any differences in the bands attributed to the sulfonate group around 1100 cm^{-1}.[33] Moreover, analysis of the spectrum indicates instead that linkage occurs through the 3,4 or 3,9 oxygen atoms, depending on the experimental conditions.[33] Figure 2 compares the ATR-IR spectrum of a TiO_2 film derivatized with AR with that obtained for the free ligand. In both cases, three different spectral regions around 1250, 1350, and 1450 cm^{-1} can be clearly distinguished. The later is dominated by C−C vibrations of the aromatic ring and does not show major differences.[12,34] On the basis of previous literature assignments[12,34] and on the result of our own IR calculations for AR at the DFT level,[35] we assigned the peak centered at 1250 cm^{-1} to the C−O stretching. It is apparent that the splitting of this band is lost upon chelation, as observed previously for catechol coupled to TiO_2.[34] Also, another similar feature between catechol and AR is that the in-plane OH bending (which according to our calculations appears at 1327 cm^{-1}) is lost upon chelation.[34] This evidence, together with the nearly identical shift observed in the UV-spectrum of A and AR upon TiO_2 complexation,[8,15] led us to conclude that the chemisorption of AR to TiO_2 occurs through the enediol group.

From a Benesi−Hildebrand analysis of the adsorption data,[8,36] we obtained the molar extinction coefficient of the complex at the absorption maximum, $\lambda = 487$ nm, $\epsilon_{487} = 9370\ M^{-1}\ cm^{-1}$, and an estimation of the association constant for the binding of AR to TiO_2, $K_{BH} = 1.5 \times 10^4\ M^{-1}$. This value is similar to that reported for other enediol ligands.[8,15]

Reactivity under Visible Irradiation. ***General Considerations.*** Stable and nonscattering sols were prepared by equilibrating 4.5 mM TiO_2 sols with 40 μM AR (Figure 1). Using the data derived from the Benesi−Hildebrand study, we calculated that only a small fraction of the dye, ca. 3%, remains free in solution and that surface coverage for TiO_2 in this system amounts to 19%.[8]

To examine the photoinduced redox behavior of the AR complex, 2.5 cm^3 of the as-prepared sols was placed in a square prismatic cell and fully illuminated with monochromatic radiation under different conditions: (a) under air saturation, (b) in the presence of chromium (VI) as acceptor, both under air and N_2-saturated atmospheres, and (c) in the presence of a sacrificial donor, hydroquinone, using dissolved O_2 as acceptor.

Photoinduced Behavior of Sols in the Absence of Added Species. Remarkably, in the absence of electron acceptors other than oxygen, the absorbance of the complex was barely affected by prolonged visible irradiation at 480 ± 5 nm. In these conditions, the complex degradation quantum efficiency is $\Phi_{-L} = (4.0 \pm 0.4) \times 10^{-4}$ for I_0 between 0.4 and 3.1 $\times$ 10^{18} s^{-1} m^{-2}. The low degradation tendency contrasts with the rapid oxidation of AR observed under visible irradiation when adsorbed on larger polycrystalline TiO_2[37,38] but is in accordance with previous qualitative investigations which indicate that other enediol ligands could hardly be oxidized by visible irradiation.[6c,8,20] Several explanations may be assayed to rationalize this behavior. It has been shown that reactive oxygen species as OH• and H_2O_2, produced after electron injection by the excited dye and the subsequent formation of superoxide radical anions (O_2^-), are essential to the degradation process of different dyes over TiO_2 Degussa P25.[37−40] For instance, it has been assessed by EPR spectroscopy that Cu^{2+} and Fe^{3+} ions, which inhibit the reduction of O_2 by conduction band electrons, simultaneously depress the degradation of sulforhodamine, alizarin red, and malachite green.[37] The restricted mobility of the ligand as a result of chemisorption may favor $AR^+ + e^-$ recombination[20] and also reduce its availability to reactive oxygen species. It is also feasible that, in contrast with the behavior observed for polycrystalline microparticles, AR^+ and O_2^- recombination prevails over AR oxidation by O_2^- in smaller domains.[41] Besides, rapid relaxation of conduction band electrons in trap states or direct electron injection into inter-band-gap states, as supported by recent theoretical and experimental evidence,[15,16] may preclude the formation of superoxide, and thus the degradation of the dye. To further analyze this hypothesis, in the following section, we explored the photoinduced reactivity of AR@TiO_2 nanoparticles in the presence of an easily reducible acceptor chromium(VI). The one-electron redox potential for

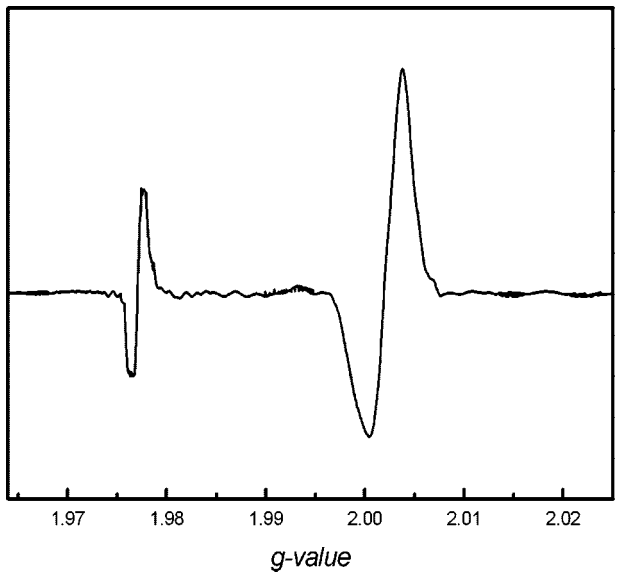

Figure 3. Transient X-band EPR spectrum obtained at room temperature upon visible irradiation ($\lambda = 470 \pm 10$ nm) of an aerated modified sol of TiO_2 nanoparticles, $[K_2Cr_2O_7]_0 = 0.1$ mM (200 μM Cr(VI)), see text.

this species, $E^0(\mathrm{Cr(VI)/Cr(V)}) = +0.55$ V,[42] is positive enough to allow its reduction by electrons trapped in inter-band-gap states.

Chromium(VI) Reduction. Previous investigations of our laboratories have shown that chromium reduction under UV excitation of naked TiO_2 particles proceeds through a single one-electron-transfer process.[43,44] In this system, chromium(V) could also be assessed as an intermediary by continuos wave EPR spectroscopy at room temperature, as indicated below. An appropriate amount of a stock solution of dichromate was added to the sol containing the modified AR@TiO_2 nanoparticles at pH 1.5, in order to give final $[\mathrm{Cr(VI)}]_0 = 200$ μM. After 15 min in the dark, an aliquot of this solution was placed in a thin quartz cylindrical tube inside the EPR cavity and then irradiated by means of a 3 W blue LED ($\lambda_{max} = 470$ nm, bandwidth = 10 nm, $I_0 = 3.3 \times 10^{19}$ s^{-1} m^{-2}). The transient spectrum obtained upon illumination is shown in Figure 3. Two paramagnetic signals at $g = 2.002$ and 1.9771, having the clear signature of an organic radical and a Cr(V) species, respectively, could be simultaneously detected. The above result is taken as evidence that some of the photogenerated electrons are effectively transferred to Cr(VI), leaving a hole in the ligand.[8,43]

Initial rates rates of Cr(VI) decay, $R_{-\mathrm{Cr(VI)}}$, were determined under monochromatic irradiation (at less than 10% of Cr(VI) conversion) as a function of chromium concentration. Quantum yields for Cr(VI) disappearance were obtained as the ratio between $R_{-\mathrm{Cr(VI)}}$ and the absorbed light intensity. The most relevant data are summarized in the first entry of Table 1, and indicate a high efficiency for chromium reduction, almost independent of the photon flux and of the irradiation wavelength, and slightly dependent on Cr(VI) concentration in the explored range, approaching a saturation value of 37% at $[\mathrm{Cr(VI)}]_0 = 200$ μM. The same results were obtained in N_2-saturated samples, confirming that O_2 does not compete with chromium for electron conduction band electrons.[43]

It is worthwhile to mention that the AR@TiO_2 system did not exhibit any reactivity in the dark, and also, no reduction of Cr(VI) could be observed upon irradiation of unmodified TiO_2 particles between 440 and 530 nm.

Figure 4 depicts the full changes in the UV−vis spectrum of the AR@TiO_2 sol obtained upon irradiation at $\lambda = 480 \pm 5$ nm, under air saturated conditions and in the presence of chromium ($[\mathrm{Cr(VI)}]_0 = 78$ μM). Figure 5 shows the results for both chromium(VI) concentration and the evolution of the absorbance at 487 nm, in the same conditions of Figure 4, as a function of the number of moles of photons absorbed per cm^3, N_p. We preferred the use of this variable, defined as $N_p = I_0 / LN_A \int_0^t (1 - 10^{-A_{480(t)}})\mathrm{d}t$ since the fraction of light absorbed by the sample is not constant, as normally found in photocatalysis, owing to the consumption of AR as irradiation proceeds. Notice that, according to the last expression, N_p would be proportional to time if A_{480} remained constant throughout the experiment. It becomes apparent that the removal of conduction band electrons by chromium species is directly linked to the destruction of the complex, since both curves in Figure 5 show the same time evolution upon irradiation.

As expected, the decay of the absorbance at 487 nm ceases when Cr(VI) has been completely reduced (see Figure 5), and conversely, complete destruction of the complex could be achieved at high Cr(VI) concentrations (data not shown). A synergistic effect on metal reduction by the presence of a oxidizable dye has previously been observed for 4-(2-hydroxy-1-naphthylazo) benzenesulfonic acid sodium salt (acid orange 7, AO7) over TiO_2 particles irradiated by visible light.[45] This behavior was ascribed to the formation of a complex between AO7 and chromium(VI). Since AR is known to chelate several metal ions,[46] a similar mechanism could be envisaged. However, we will show in the following that the behavior observed in this case has a different origin.

TABLE 1: Initial Quantum Yields for Chromium(VI) Disappearance, $\Phi_{-\mathrm{Cr(VI)}}$, in AR@TiO_2 and Cr(VI)@TiO_2 Systems

system[a]	$[\mathrm{Cr(VI)}]_0$ (μM)	λ (nm)	$10^{18} \times I_0$ (s^{-1} m^{-2})	$100 \times \Phi_{-\mathrm{Cr(VI)}}$
AR@TiO_2	40	480	0.85	14.5 ± 1
	200	480	0.42	37 ± 3
	200	480	3.10	35 ± 2
	200	530	1.02	36 ± 2
Cr(VI)@TiO_2	200	303	4.80	5.0 ± 0.5
	200	400	4.80	2.5 ± 0.3

[a] All the determinations were done at room temperature, in aqueous sols at pH 1.5, $[TiO_2] = 4.5$ mM, at the irradiation wavelength $\lambda \pm 5$ nm.

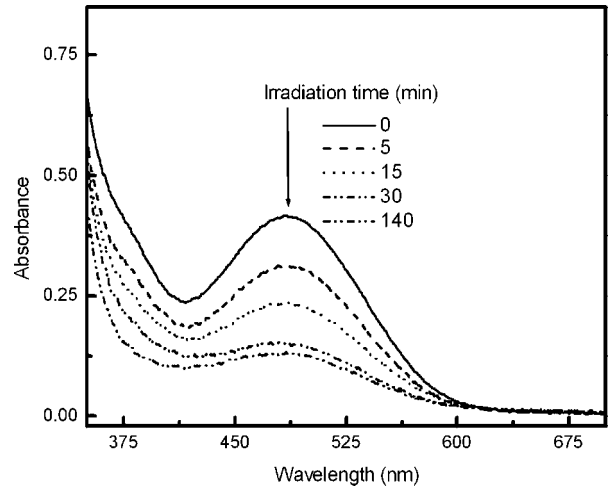

Figure 4. Changes in the UV−vis spectra of an AR@TiO_2 sol obtained after irradiation at $\lambda = 480 \pm 5$ nm, in the presence of chromium ($[\mathrm{Cr(VI)}]_0 = 78$ μM, pH 1.5). The arrow indicates the decay in the absorbance of the AR@TiO_2 charge-transfer band, which ceases after complete Cr(VI) reduction.

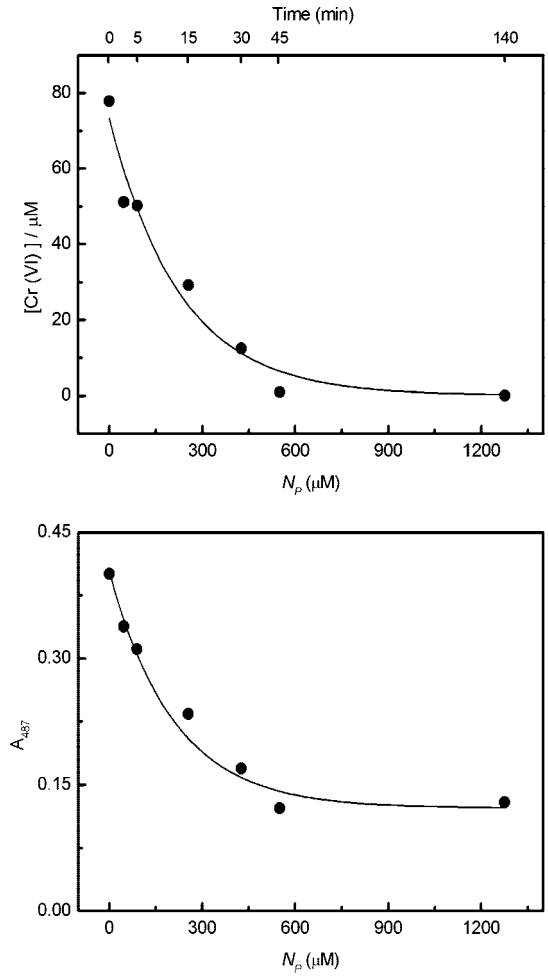

Figure 5. [Cr(VI)] profile and absorbance of the complex at 487 nm as a function of the number of absorbed photons, N_p, see text. The top axis in the upper figure shows the irradiation time. Conditions as in Figure 4.

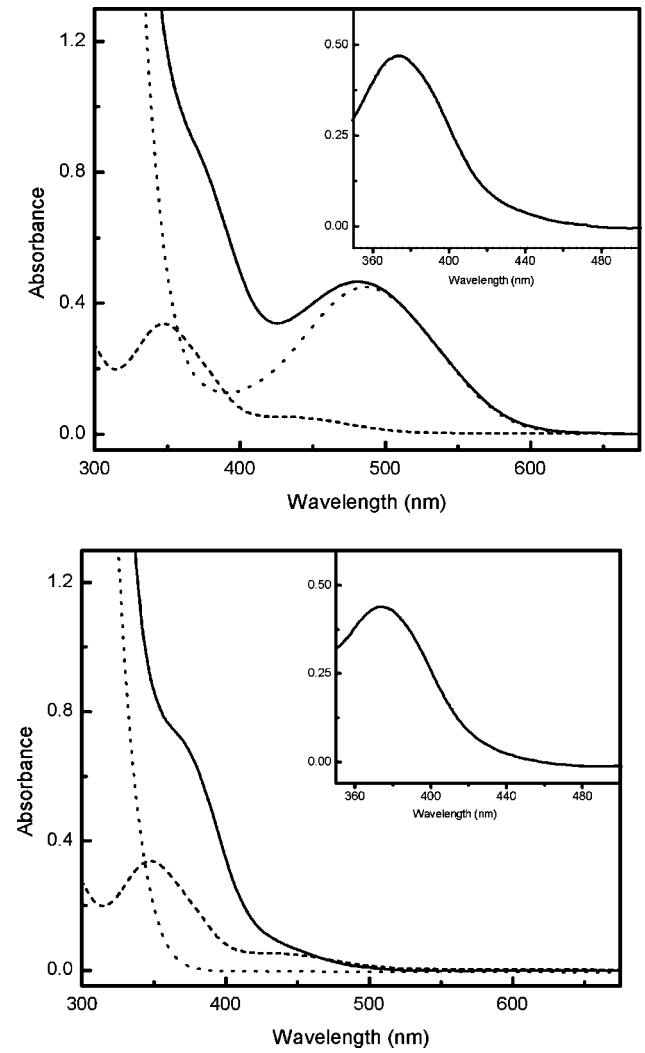

Figure 6. Upper panel: UV−vis absorption spectra of: 4.5 mM sol of TiO_2 particles modified with 40 μM AR, (---); 200 μM aqueous solution of Cr(VI), pH 1.5 (•••); and (—) a 4.5 mM sol of TiO_2 particles modified with 40 μM AR after the addition of 200 μM Cr(VI). The inset shows the difference between the solid curve and the arithmetic sum of the dashed and dotted line.

To begin with, it is interesting to point out that the UV−vis spectrum resulting from the mixture of a solution of chromium(VI) with a previously modified sol of AR@TiO_2 particles does not result in the simple sum of its components, as shown in the upper graph of Figure 6. The difference between the actual spectrum of the mixture and the spectra of the Cr(VI) solution plus the AR@TiO_2 sol is displayed in the inset. Instead of the characteristic band in the visible region reported for other complexes of AR with metal ions, the spectrum in the inset shows a maximum at 375 nm and a tailoring absorbance that extends up to 430 nm.[46] Moreover, we observe that the addition of a Cr(VI) solution to a sol of naked TiO_2 particles produces a similar shift in the spectrum of the TiO_2 sol to the visible region with an apparent shoulder at 375 nm, as displayed in the lower graph of Figure 6. The inset of this graph shows the result of subtracting the spectrum obtained by the simple sum of the spectra of the TiO_2 sol and the Cr(VI) solution to that of the corresponding mixture. In view of the perfect coincidence of the results in both insets, we assign this spectrum to a charge-transfer complex between TiO_2 and chromium(VI), hereafter denoted as Cr(VI)@TiO_2. The complex has previously been investigated by ATR-IR spectroscopy;[47] however, to our knowledge, this is the first report on its UV characterization.

Moreover, the addition of AR to a sol of Cr(VI)@TiO_2 produces the instantaneous coupling of alizarin red to TiO_2, with no changes in the band at 375 nm. That is, chelation of TiO_2 particles with both the enediol ligand and Cr(VI) results in the same spectrum independent of whether the mixtures are prepared by adding first Cr(VI) to the sol of AR@TiO_2 nanoparticles or AR to a Cr(VI)@TiO_2 sol, with no visible signs of Cr(VI)−AR interaction.

Nevertheless, we were able to detect the slow formation of a complex between Cr(VI) and AR in the absence of TiO_2. We observe that the addition of Cr(VI) to a 40 μM AR solution slowly shifts its spectrum to the red. At the highest chromium concentration used in this work, $[Cr(VI)]_0 = 200$ μM, the mixture requires more than two hours to fully equilibrate, and the final spectrum displays a maximum at $\lambda_m = 465$ nm ($A_{465} = 0.14$). However, no decay in Cr(VI) concentration in A_{465} could be detected after prolonged excitation of this band by visible light; i.e., the mixture of AR and chromium does not show any reactivity in the absence of TiO_2.[48] Thus, we conclude that, after AR excitation, the electron is injected into TiO_2 nanoparticles and then transferred to the Cr(VI) ions chelating the surface. The strong interaction between Cr(VI) and valence-unfilled Ti(IV) atoms at the TiO_2 surface, together with the favorable redox potential of the couple Cr(VI)/Cr(V),[42] is proposed as the rationale for the high efficiency of charge

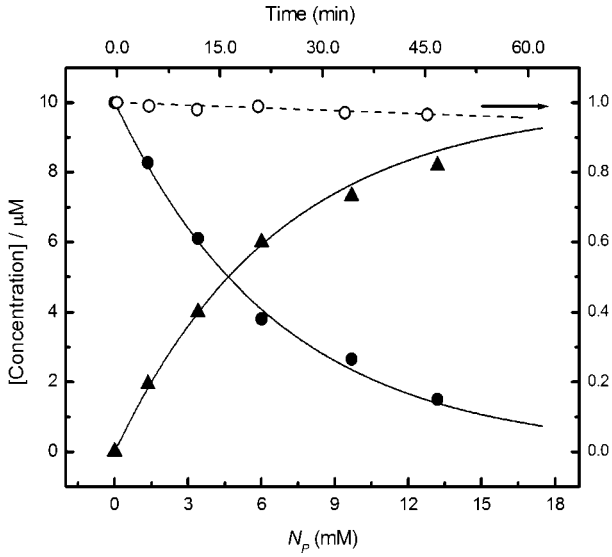

Figure 7. HQ (●) and BQ (▲) concentrations as a function of the number of absorbed photons and time, obtained upon irradiation at $\lambda = 480 \pm 5$ nm, $I_o = 2.92 \times 10^{19}$ s^{-1} m^{-2}. Dashed line corresponds to the relative changes in the absorbance of the complex at 487 nm, right axis.

utilization. For comparative purposes, we determined the initial quantum yields of chromium disappearance in aqueous sols of Cr(VI)@TiO_2 nanoparticles at pH 1.5 in the absence of the dye, at two different wavelengths, 400 and 303 nm, selectively exciting the Cr(VI)@TiO_2 charge-transfer band or the semiconductor, respectively. The values listed in Table 1 indicate that the reduction of 200 μM Cr(VI) by visible irradiation (480 nm) in AR@TiO_2 sols is far more efficient ($\Phi_{-Cr(VI)} = 37\%$) than that produced by exciting the semiconductor ($\Phi_{-Cr(VI)} = 5\%$), or the charge-transfer band at 400 nm ($\Phi_{-Cr(VI)} = 2.5\%$), all determined at the same [TiO_2] and I_0.

Hydroquinone Oxidation. As normally found in dye−TiO_2 coupled systems, the oxidative power of AR@TiO_2 system is expected to be considerably inferior to that obtained by direct UV excitation of the naked semiconductor, since it is limited by the redox potential of the dye radical cation.[49] For free AR in acetonitrile, we determined a value of 1.5 V versus NHE. Considering this figure, we assayed phenol and hydroquinone (HQ) as possible sacrificial donors, whose one-electron redox potentials at pH 1.5 are 0.77 and 1.1 V, respectively.[49] We found that only hydroquinone could be transformed with a measurable efficiency. As illustrated in Figure 7, using only oxygen as acceptor, the oxidation of HQ proceeded stoichiometrically to benzoquinone, BQ, with no visible changes in the charge-transfer band of the AR@TiO_2 complex. A low efficiency $\Phi_{-HQ} = 0.3\%$ could be calculated for $10 \leq [HQ]/\mu M \leq 100$.

Conclusions

The photochemical behavior of the coupled system AR@TiO_2 was analyzed through determinations of initial quantum yields in nonscattering sols of TiO_2 modified nanoparticles. Visible photoinduced oxygen reduction in this system proceeds with very low efficiency, as inferred by the high stability of the ligand in the absence of added acceptors or donors. In addition, only easily oxidizable donors such as hydroquinone could be transformed by AR, with measurable efficiency. Nevertheless, chromium(VI) scavenges most of the electrons injected into TiO_2. In addition, we report for the first time the UV−vis characterization of a Cr(VI)−TiO_2 surface complex, and demonstrated that chromium(VI) could be reduced by sub-band-gap irradiation at $\lambda = 400$ nm. The strong interaction between Cr(VI) and TiO_2 particles observed at acidic pH is also of interest in the UV-induced TiO_2 photocatalytic systems, and may contribute to understand why Cr(VI) reduction is not inhibited by oxygen, in contrast with the behavior observed for other metals ions like Hg(II) or Pb(II).[44,50]

Our results are particularly relevant to the characterization of nanoparticulate systems. Molecular adsorption of AR and Cr(VI) may predominate over chelation in larger particles, exposing less undercoordinated Ti sites at the interface, and hide the behavior of chemisorbed species, which are directly scrutinized in this work.

Acknowledgment. The authors are in debt to Dr. Marta Brusa for her able assistance with the EPR measurements. This work was financially supported by the National Research Council of Argentina, CONICET, PIP 5472 project. E.S.R., M.I.L., and M.A.G. are members of CONICET. Y.D.I. thanks CONICET for a doctoral fellowship.

References and Notes

(1) *Semiconductor Photochemistry and Photophysics: Molecular and Supramolecular Photochemistry*; Ramamurthy, V., Schanze, K. S. , Eds.; Marcel Dekker: New York, 2003.

(2) Hebda, M.; Stochel, G.; Szacilowski, K.; Macyk, W. *J. Phys. Chem. B* **2006**, *110*, 15275–15283.

(3) Argazzi, R.; Murakami Iha, N. Y.; Zabri, H.; Odobel, F.; Bignozzi, C. A. *Coord. Chem. Rev.* **2004**, *248*, 1299–1316.

(4) Durrant, J. R.; Haque, S. A.; Palomares, E. *Coord. Chem. Rev.* **2004**, *248*, 1247–1257.

(5) (a) Tae, E. L.; Lee, S. H.; Yoo, S. S.; Kang, E. J.; Yoon, K. B. *J. Phys. Chem. B* **2005**, *109*, 22513–22522. (b) Mosurkal, R.; He, J.-A.; Samuelson, L. A.; Kumar, J. *J. Photochem. Photobiol., A* **2005**, *168*, 191–196.

(6) (a) Frei, H.; Fitzmaurice, D.; Grätzel, M. *Langmuir* **1990**, *6*, 198–206. (b) Moser, J.-E.; Punchihewa, S.; Infelta, P. P.; Grätzel, M. *Langmuir* **1991**, *7*, 3012–3018. (c) Houlding, V. H.; Grätzel, M. *J. Am. Chem. Soc.* **1983**, *105*, 5695–5696.

(7) Redmond, G.; Fitzmaurice, D. *J. Phys. Chem.* **1993**, *97*, 6951–6954.

(8) Rajh, T.; Chen, L. X.; Lukas, K.; Liu, T.; Thurnauer, M. C.; Tiede, D. M. *J. Phys. Chem. B* **2002**, *106*, 10543–10552.

(9) (a) Dimitrijevic, N. M.; Saponjic, Z. V.; Bartels, D. M.; Thurnauer, M. C.; Tiede, D. M.; Rajh, T. *J. Phys. Chem. B* **2003**, *107*, 7368–7375. (b) De la Garza, L.; Saponjic, Z. V.; Dimitrijevic, N. M.; Thurnauer, M. C.; Rajh, T. *J. Phys. Chem. B* **2006**, *110*, 680–686.

(10) (a) Rajh, T.; Nedeljkovic, J. M.; Chen, L. X.; Poluekotov, O.; Thurnauer, M. C. *J. Phys. Chem. B* **1999**, *103*, 3515–3519. (b) Makarova, O. V.; Rajh, T.; Thurnauer, M. C.; Martin, A.; Kemme, P. A.; Cropek, D. *Environ. Sci. Technol.* **2000**, *34*, 4797–4803. (c) Rajh, T.; Ostafin, A. E.; Micic, O. I.; Tiede, D. M.; Thurnauer, M. C. *J. Phys. Chem.* **1996**, *100*, 4538–4545.

(11) (a) Agrios, A. G.; Gray, K. A.; Weitz, E. *Langmuir* **2003**, *19*, 1402–1409. (b) Kim, S.; Choi, W. *J. Phys. Chem. B* **2005**, *109*, 5143–5149.

(12) Lana-Villarreal, T.; Rodes, A.; Perez, J. M.; Gomez, R. *J. Am. Chem. Soc.* **2005**, *127*, 12601–12611.

(13) (a) Cho, Y.; Kyung, H.; Choi, W. *Appl. Catal., B* **2004**, *52*, 23–32. (b) Paul, T.; Miller, P. L.; Strathmann, T. J. *Environ. Sci. Technol.* **2007**, *41*, 4720–4727.

(14) (a) Hug, S. J.; Sulzberger, B. *Langmuir* **1994**, *10*, 3587–3597. (b) Tunesi, S.; Anderson, M. A. *Langmuir* **1992**, *8*, 487–495. (c) Araujo, P. Z.; Mendive, C. B.; García Rodenas, L. A.; Morando, P. J.; Regazzoni, A. E.; Blesa, M. A.; Bahnemann, D. *Colloids Surf., A* **2005**, *265*, 73–80.

(15) Huber, R.; Sporlein, S.; Moser, J.-E.; Grätzel, M.; Wachtveitl, J. *J. Phys. Chem. B* **2000**, *104*, 8995–9003.

(16) Huber, R.; Moser, J.-E.; Grätzel, M.; Wachtveitl, J. *J. Phys. Chem. B* **2002**, *106*, 6494–6499.

(17) Ramakrishna, G.; Singh, A. K.; Palit, D. K.; Ghosh, H. N. *J. Phys. Chem. B* **2004**, *108*, 1701–1707.

(18) Wang, Y.; Hang, K.; Anderson, N. A.; Lian, T. *J. Phys. Chem. B* **2003**, *107*, 9434–9440.

(19) Grela, M. A.; Colussi, A. J. *J. Phys. Chem. B* **1999**, *103*, 2614–2619.

(20) Tachikawa, T.; Takai, Y.; Tojo, S.; Fujitsuka, M.; Majima, T. *Langmuir* **2006**, *22*, 893–896.

(21) Minero, C.; Mariella, G.; Maurino, V.; Pelizzetti, E. *Langmuir* **2000**, *16*, 2632–2641.

(22) (a) Rego, L. G. C.; Batista, V. S. *J. Am. Chem. Soc.* **2003**, *125*, 7989–7997. (b) Duncan, W. R.; Stier, W. M.; Prezhdo, O. V. *J. Am. Chem. Soc.* **2005**, *127*, 7941–7951. (c) Stier, W.; Duncan, W. R.; Prezhdo, O. V. *Adv. Mater.* **2004**, *16*, 240–244. (d) Duncan, W. R.; Craig, C. F.; Prezhdo, O. V. *J. Am. Chem. Soc.* **2007**, *129*, 8528–8543.

(23) Perrin, D. D.; Armarego, W. L. F. *Purification of Laboratory Chemicals*; Pergamon Press: Oxford, 1988; pp 131.

(24) Wegner, E. E.; Adamson, A. W. *J. Am. Chem. Soc.* **1966**, *88*, 394–404.

(25) (a) Kormann, C.; Bahnemann, D. W.; Hoffmann, M. R. *J. Phys. Chem.* **1988**, *92*, 5196–5201. (b) Draper, R. B.; Fox, M. A. *Langmuir* **1990**, *6*, 1396–1402.

(26) Weng, Y.-X.; Wang, Y.-Q.; Asbury, J. B.; Ghosh, H. N.; Lian, T. *J. Phys. Chem. B* **2000**, *104*, 93–104.

(27) Choi, W.; Termin, A.; Hoffmann, M. R. *J. Phys. Chem.* **1994**, *98*, 13669–13679.

(28) Brusa, M. A.; Di Iorio, Y.; Churio, M. S.; Grela, M. A. *J. Mol. Catal. A: Chem.* **2007**, *268*, 29–35.

(29) (a) Defoin, A.; Defoin-Straatmann, R.; Hildenbrand, K.; Bittersmann, E.; Kreft, D.; Kuhn, H. J. *J. Photochem.* **1986**, *33*, 237. (b) Kuhn, H. J.; Görner, H. *J. Phys. Chem.* **1988**, *92*, 6208.

(30) (a) Hatchard, C. G.; Parker, C. A. *Proc. R. Soc.* **1956**, *235A*, 518–536. (b) Kirk, A. D.; Namasivayan, C. *Anal. Chem.* **1983**, *55*, 2428–2429.

(31) *Standard Methods for the Examination of Water and Wastewater*, 20th ed.; Clesceri, L. S.; Greenberg, A. E.; Eaton A. D., Eds.; American Public Health Association: Washington, DC, 1998.

(32) (a) Shoute, L. C. T.; Loppnow, G. R. *J. Chem. Phys.* **2002**, *117*, 842–850. (b) Redfern, P. C.; Zapol, P.; Curtiss, L. A.; Rajh, T.; Thurnauer, M. C. *J. Phys. Chem. B* **2003**, *107*, 11419–11427. (c) Duncan, W.; Prezhdo, O. V. *J. Phys. Chem. B* **2005**, *109*, 365–363.

(33) Jayaweera, P. M.; Jayarathne, T. A. U. *Surf. Sci.* **2006**, *600*, L297−L300.

(34) Araujo, P. Z.; Morando, P. J.; Blesa, M. A. *Langmuir* **2005**, *21*, 3470–3474.

(35) The IR spectra was calculated at the DFT level of theory using the three-parameter exchange functional of Becke B3LYP and 6−31++G(d) basis set as implemented in the SPARTAN '04 package, Wavefunction Inc.

(36) Ramakrishna, G.; Ghosh, H. N.; Singh, A. K.; Palit, D. K.; Mittal, J. P. *J. Phys. Chem. B* **2001**, *105*, 12786–12796.

(37) Chen, C.; Li, X.; Ma, W.; Zhao, J.; Hidaka, H.; Serpone, N. *J. Phys. Chem. B* **2002**, *106*, 318–324.

(38) Liu, G.; Li, X.; Zhao, J.; Horikoshi, S.; Hidaka, H. *J. Mol.Catal. A: Chem.* **2000**, *153*, 221–229.

(39) (a) Wu, T.; Liu, G.; Zhao, J.; Hidaka, H.; Serpone, N. *J. Phys. Chem. B* **1999**, *103*, 4862–4867. (b) Liu, G.; Zhao, J.; Hidaka, H. *J. Photochem. Photobiol., A* **2000**, *133*, 83–88.

(40) Yang, J.; Chen, C.; Ji, H.; Ma, W.; Zhao, J. *J. Phys. Chem. B* **2005**, *109*, 21900–21907.

(41) Biancardo, M.; Argazzi, R.; Bignozzi, C. *Inorg. Chem.* **2005**, *44*, 9619–9621.

(42) Niki, K. In *Standard Potentials in Aqueous Solutions*; Bard, A., Parsons, R. , Jordan, J., Eds.; Marcel Dekker, Inc.: New York, 1985; Chapter 16, p 461.

(43) (a) Testa, J. J.; Grela, M. A.; Litter, M. I. *Langmuir* **2002**, *17*, 3515–3517. (b) Testa, J. J.; Grela, M. A.; Litter, M. I. *Environ. Sci. Technol.* **2004**, *38*, 1589–1594. (c) Meichtry, J. M.; Brusa, M.; Mailhot, G.; Grela, M. A.; Litter, M. I. *Appl. Catal., B* **2007**, *71*, 101–107.

(44) Litter, M. I. *Appal. Catal., B* **1999**, *23*, 89–114.

(45) Kyung, H.; Lee, J.; Choi, W. *Environ. Sci. Technol.* **2005**, *39*, 2376–2382.

(46) (a) Das, S.; Saha, A.; Mandal, P. C. *Talanta* **1996**, *43*, 95–102. (b) Nejati-Yazdinejad, M. *Anal. Sci.* **2006**, *22*, 617–619. (c) Bilgic, D.; Karaderi, S.; Bapli, I. *Rev. Anal. Chem.* **2007**, *26*, 99–108.

(47) García Rodenas, L. A.; Weisz, A. D.; Magaz, G. E.; Blesa, M. A. *J. Colloid Interface Sci.* **2000**, *230*, 181–185.

(48) Using the value of the formation constant for the metal complex of Cr(VI) with alizarin red reported in Table 8.13 of *Lange's Handbook of Chemistry*, 14th ed.; Dean, J., Ed.; McGraw-Hill, Inc.: New York, log $K_f = 4.7$, we calculated that, after equilibration of this mixture, only 10% of the initial AR remains free $[AR]_{eq} \approx 4\ \mu M$.

(49) Hodak, J.; Quinteros, C.; Litter, M. I.; San Román, E. *J. Chem. Soc. Faraday Trans.* **1996**, *92*, 5081–5088.

(50) (a) Botta, S. G.; Rodríguez, D. J.; Leyva, A. G.; Litter, M. I. *Catal. Today* **2002**, *76*, 247–258. (b) Murruni, L.; Leyva, G.; Litter, M. I. *Catal. Today* **2007**, *129*, 127–135.

JP8040742